Machine learning impassioned assessment of trap states driven band bending analysis in organic Schottky formation

Kushal Chakraborty [a,*], V. Chandrasekar [a,*], Dhananjay Kumar [b], Nabin Baran Manik [c]

[a] Department of CSE-AI/ML, Jain University, Karnataka 562121, India
[b] Department of CSE-Cyber Security, Jain University, Karnataka 562121, India
[c] Department of Physics, Jadavpur University, Kolkata 700032, India

ARTICLE INFO

ABSTRACT

Band bending at metal–semiconductor junction bears significant consequences providing analytical explanation of built-in-voltage (V_{bi}) in current–voltage (I-V) relationship. Knowing the band bending impact on charge transition, a theoretical model has been developed which relates the parameter with geometrical conductance (g_m) by introducing modification in empirical Mott-Gurney law. The theoretical relation is validated with the approximated outcome of organic semiconductor-based prototype simulated device structure ranges between 100 nm to 900 nm. The same has been examined on two different experimental semiconducting dye based organic diode. For each case, the result reveals a greater range of consistency satisfying a well trend of analogy with theoretically developed equation. Band bending (b) shows inverse linearity with g_m at increasing voltage, whereas the following investigation explore its proportional nature with increasing device thickness (L). Since organic materials are trap prone and its influence on charge conduction is well known, therefore, to predict the impact of trap distributions on b, machine-learning based modeling approaches has been undertaken to leverage the prediction in a reliable way to quantify the trap energy (E_T). The comparison among different output set of computational modelling approach leads towards a non-linear approximation of b with variation of E_T and is best applicable at 700 nm device thickness. Furthermore, different linear and non-linear Machine Learning algorithm has been trained for validation employing the considered sample thickness in experimental dye-based devices and based on the assessment of performance metrics, the influence of E_T on variation of b has been detected.

1. Introduction

Estimation of space charge limited conduction (SCLC) relies on the analysis of I-V characteristics of single-carrier devices. Simplification of this SCLC measurement produces it as a convenient avenue for investigation over the properties relative to the mechanism of charge transport into organic semiconductors [1,2]. Moreover, this permits a direct comparison on variation of thickness of sample films utilized for determination of optoelectronic parameters and charge transport. The following process in contrast to other renowned methodology such as time of flight (TOF) technique, field effect transistor (FET) measurement technique which require marginal sample thickness level and lateral device nature and hence probe the lateral impact of charge transition. Therefore, single carrier devices of different sample thickness are taken into consideration for the following investigation. Work function difference of the electrodes used in the device leads towards the interfacial

band bending during the charge transformation by execution of externally applied voltage [3–5]. Interfacial band-bending plays an important role to understand the device performance in different high mobility semiconducting organic molecules. Organic material/electrodes interfacial mismatch was obtained to be a crucial consideration in single charge conduction across the interface such as carrier injection and extraction of carriers in optoelectronic configurations. Such misalignment in energy level has extensively been argued in different reports [6–8]; several proposals have been offered to have a better insight on the physics of interfacial transition. So far, devices based on organic semiconductors still depend upon the explanation regarding intrinsic behavior of organic molecules and eventually, interfacial transition have not been studied vastly to gain a clear conception on the working function of such devices. Therefore, meaningful tailoring of interfacial band bending parameter might be effective to explore the desired explanation by filling up the flaws related to above mentioned

challenge. Tuning on band bending could also be possible in presence of different substrates having certain work function differences. In case of such asymmetric work functions between the electrodes, existence of a built-in voltage (V_{bi}) can be observed [9]. For voltages working below V_{bi}, diffusion of charges takes place whereas drift dominated current conduction occurs above V_{bi} [10]. SCLC current can be approximated at drift current regime for an ohmic injection without traps and is given by empirical Mott-Gurney law (Fig. 1):

$$J = \frac{9}{8} \epsilon \epsilon_0 \mu \frac{(V - V_{bi})^2}{L^3} \qquad (1)$$

where J is the current density, ϵ is the permittivity, μ is the carrier mobility and L is sample layer thickness. The equation is well suited for high voltage regime where $V > V_{bi}$. V_{bi} can be estimated by different measurement techniques like electro-absorptions method [11], photo-electronic measurement [12], estimation of voltage-capacitance analysis [13]. But the processes are not very accurate so far in all cases [14]. Hence, a technique has been undertaken in present report where the measurement has been interpreted by analyzing I-V plot. The method is reliable while band bending at injection level are taken into account. Band bending has significant influence on determination of V_{bi} and subsequently, approximation of charge carrier mobility. By accounting for the following technique, a nearly suitable agreement has been obtained between simulation result and theoretically fitted modeling. Extraction of band bending (b) and V_{bi} accordingly by utilizing proposed method related to direct approximation of SCLC conduction based I-V plot indicates the importance of both parameters. The findings of the investigation are applicable in variable film thickness with relatively large metal–semiconductor interfacial injection for almost all organic semiconductors. On the other hand, since organic semiconductors are prone to traps due to their disordered nature, therefore, trap energy based disordered states can be encountered during charge conduction. Conducting carriers faces challenge in frequent movement in such arbitrarily oriented shallow and deep level of trap distributions. A clear expectation should be encouraged to find out the probable impact of trapping states on band bending. No direct theoretical model has been approximated so far which predicts the trap energy (E_T) influences on b. Machine learning (ML) based assessment might be a popular choice in this regard which potentially predict the complex model of relationships between these two elementary parameters [15,45]. In absence of huge number of training data-set, mathematical execution might be possible in such cases to demonstrate the properties of devices [15,42,43]. An experimentally validated data-set is able to train ML prediction to resolve the complexity and perhaps for the first time the thought has been implemented in present investigation. Earlier, Padula et al. [16], demonstrated photovoltaic estimations of 249 organic molecules by introducing k-NN regression [17] and kernel-ridge regression [18,19] method, predicted different electro-structural properties. Sahu et al [20] utilized RF (Random Forest) and GB (Gradient Boosting) approximation to estimate the device efficiency for nearly 280 OPV materials utilizing 13 elemental microscopic characteristics to train the respective models. Pereira et al [21] determined the band gap energy between HOMO-LUMO gap of different energy materials using ML approach. They obtained that RF trained model was best suited on the basis of descriptor produced best predictions for HOMO-LUMO energy gap. In present report, a non-linear relationship has been predicted between E_T and b at different sample thickness ranges between 100 nm to 900 nm by analysing different linear/ non-linear ML model approximation. The
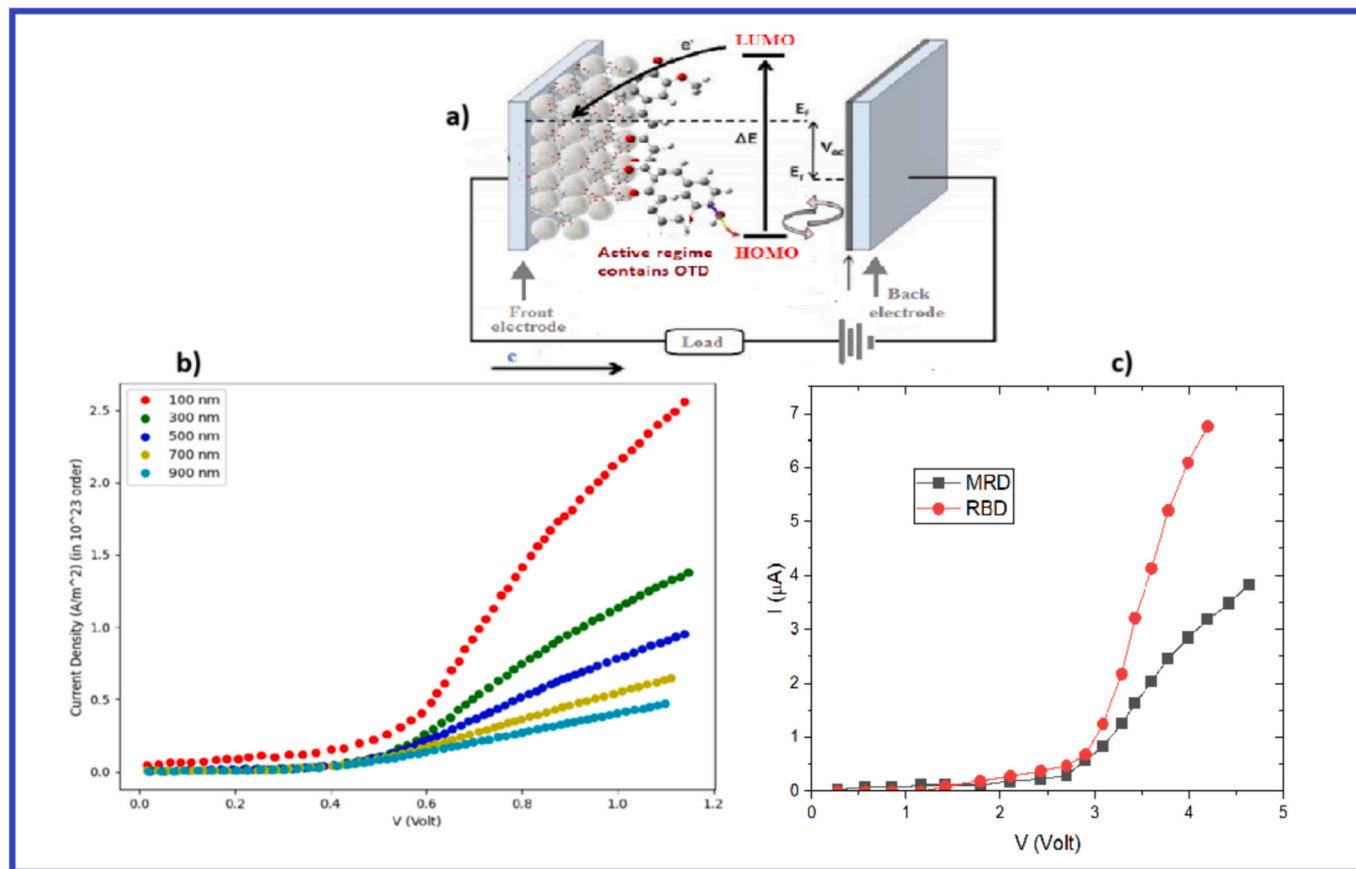

Fig. 1. (a) schematic design of device arrangement and charge transformation in organic dye-based schottky device, (b) simulated I-V characteristics of organic schottky contact compiled in Oghma-nano modelling technique and plotted in python for 100 nm, 300 nm, 500 nm, 700 nm and 900 nm sample layer thickness, (c) experimental outcome containing I-V plot of RBD (Rose Bengal Dye) and MRD (Methyl Red Dye) based organic diode.

following analysis would be fruitful for enrichment of knowledge regarding the designing of applications of different organic molecule in optoelectronic devices (Table 1).

2. Methods and techniques

2.1. Simulation technique

One reliable and well-known simulation approach named as Oghma-Nano (GPVDM) technique [22,23], used for implementation of critical optoelectronic device structures modeling, have been used to extrapolate of I-V plot at different layer thickness. Divisions are set to obtain the consistent outcome at different sample thickness ranges between 100 nm to 900 nm. All the relevant parameters are considered on the basis of earlier reported standard value in the following simulation for compilation of the reliable execution of modeling such as follows: charge mobility (μ), effective charge density (N_v), Rechardson Constant (A^*), free electron to trapping electron ratio ($n_{e,f}$), trapping density (N_t), free hole to trapped hole ratio ($h_{e,f}$), trapping electron to free electron ratio ($n_{e,t}$), trapping hole to free hole ratio ($h_{e,t}$), characteristic temperature (T_c) are 4.96×10^{-7} m^{2}V^{-1}s^{-1}, 3.8×10^{26} cm^{-3}, 5.4×10^{-4} A/m^{2}K^2, 2.50×10^{-20} m^{-2}, 1.45×10^{25} m^{-3}eV^{-1}, 4.67×10^{-26} m^{-2}, 1.32×10^{-22} m^{-2}, 4.86×10^{-22} m^{-2}, 1200 K respectively. Data containing the output graph has subsequently plotted in Origin pro 9.0 software.

2.2. Experimental methodology

10 gm of experimental dyes- Rose Bengal dye (abbreviated as RBD) and Methyl Red dye (abbreviated as MRD), mixed with ethanol solution has been stirred well to make its homogeneous solution at 60∘ temperature for 3 h. The prepared solution is kept next 30 mins to form a homogeneous concentration. Al and Cu are then cleaned for 10 mins introducing ultrasonic cleaning technique. In next step, the substrates are etched with HF/H$_2$O at 1:10 ratio. Hence the solution is placed by spin-coating technique on front electrode (Al) and back electrode (Cu) by using spin coating method with a speed of 1000 rpm. 5.5×10^5 mbar has been maintained during the deposition process. The electrodes are merged together and left it for 1 h for the formation of the Schottky contact. The voltage and current are estimated with Keithley 6½ digit multimeter, model number 2000. However, further detail of the sample materials, device preparation and experimental devices specification has been discussed in our earlier report [24]. (Materials description has been given in Supplementary File- Pt.1.).

2.3. Machine learning based approach

We have introduced computational method to study the relationship between the E_T and b for the simulated Schottky device structure contained data for different thickness. We have trained multiple linear and non-linear machine learning models to understand the relationship between E_T and b. Finally, we used the model pre-trained over simulated data to predict the output values (b) for experimental outcome.

3. Result and discussion

In schematic representation of b in Fig. 2, the zero-injection barrier leads to a sharp bending across the vicinity of the back electrode (cathode) due to the accumulation of diffused charges. The barrier ϕ_b anode has a non-zero value and gradually there is signature of b across the regime of this electrode. A built-in potential (V_{bi}) having a resultant value of (ϕ_b-b) can be encountered in quasi-flat band condition. This emphasizes on the classical relevance of band-bending at the point of injection contact for internal field generation in the interfacial regime. Inclusion of b is effective not only for correct elucidation of V_{bi} but equally crucial for charge transition in forward bias mode.

3.1. Analytical discussion over experimental and simulation-based outcomes

Notably, the MG law regarding charge transformation mentioned in Eq. (1) is not suitable in reverse bias due to non-ohmic nature of injection regime that restricts the formation of barrier of space charge. The accurate explanation of the following I-V relationship defined by the abovesaid law is well applicable for forward bias charge transition where the contribution of both diffusion current and drift current is precisely interpreted. The analogy of the consideration has been implemented both in simulation result obtained at different sample layer thickness and experimental outcome of two different organic dye based Schottky contact which exhibits a high range of consistency together in present investigation. Accumulated observation of drift–diffusion conduction has been fitted to find out the variation of V_{bi} and b with sample thickness. V_{bi} results horizontal shifting of conduction towards exponential SCLC regime. In present report, V_{bi} is estimated from the transition diffusion regime to quadratic drift regime in semi-log I-V relationship. Greater range of similarity over the trends of d(lnI)/dV-V plot in both simulated and experimental devices exhibits the validity of the technique under consideration and that has been expressed in
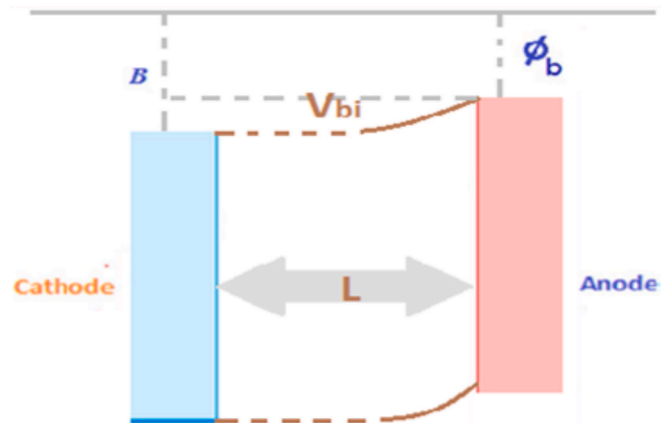

Fig. 2. Schematic presentation of band bending during charge transition of organic semiconductor based Schottky contact.

Table 1
Estimated value of b, V_{bi} and ϕ_b at different sample thickness and organic dye-based devices.

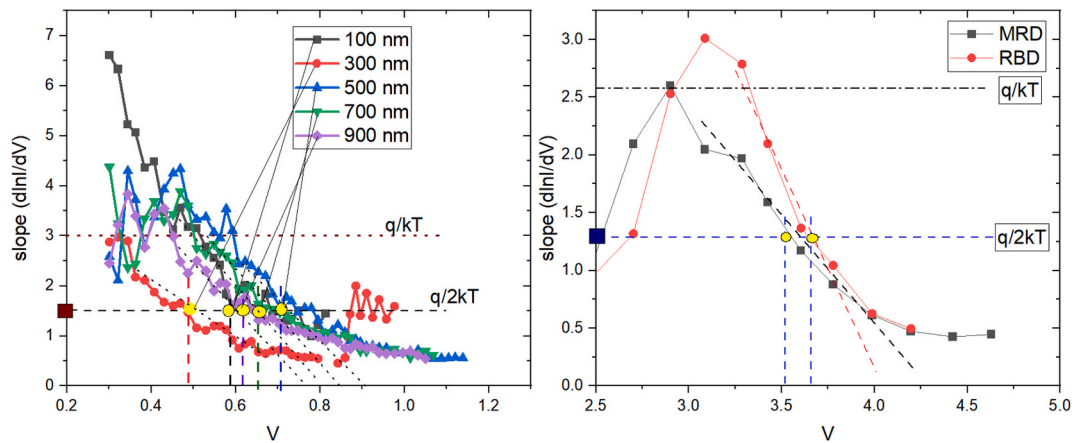| Simulation results (Thickness [L] variation)					Experimental results (Material variation)			
L(nm)	b (eV)	V_{bi}(Volt)	ϕ_b(eV)		Organic dye	b(eV)	V_{bi}(Volt)	ϕ_b(eV)
100	0.242	0.58	0.82		MBD	2.53	3.52	0.99
300	0.298	0.49	0.79		RBD	2.68	3.63	0.95
500	0.325	0.70	1.02					
700	0.343	0.64	0.98					
900	0.356	0.61	0.96					

Fig. 3. d(lnI)/dV-V plot for (a) numerical simulated Schottky contact at 100 nm, 300 nm, 500 nm, 700 nm, 900 nm sample thickness, (b) experimental dye based Schottky contact for RBD and MRD organic device. The coinciding point of voltage and slope of the derivative over q/2kT dashed line (estimated by yellow circle on point of intersect and coloured square marked on vertical axis) signifies the value of V_{bi} from which ϕ_b can be calculated.

Fig. 3.

In the level of below V_{bi}, the slope in Fig. 3 approaches to (q/kT). With increasing voltage, reduction in steepness of the slope can be observed in transition regime of drift–diffusion domain [25,26,44]. Trend of the slope achieves nearly the value of (q/2kT) at the point of transition. The differential value of d(lnI)/dV of the analytical drift–diffusion conduction approaches (q/2kT) where the applied voltage meets to V_{bi} that leads to the confirmation of slope transition corresponds to the V_{bi}. The estimated value of ϕ_b from the slope estimation for both simulated and experimental device structures shows

high similarities expressing the reliability of the following analogy under consideration. (Also see the Supplementary File- Pt.2 where geometrical conductance shows almost similar trends at higher voltage for all sample thickness.).

On the other hand, electrostatic model focusing on the perspective of band-bending interprets the dependence of ϕ_b on b with Fermi level shifting. The modeling could be applicable more according to the work function difference of device electrodes. Low work function offers high state of Fermi level. Electrons start flowing from high fermi level towards low Fermi level states upon formation of contacts and holes follow
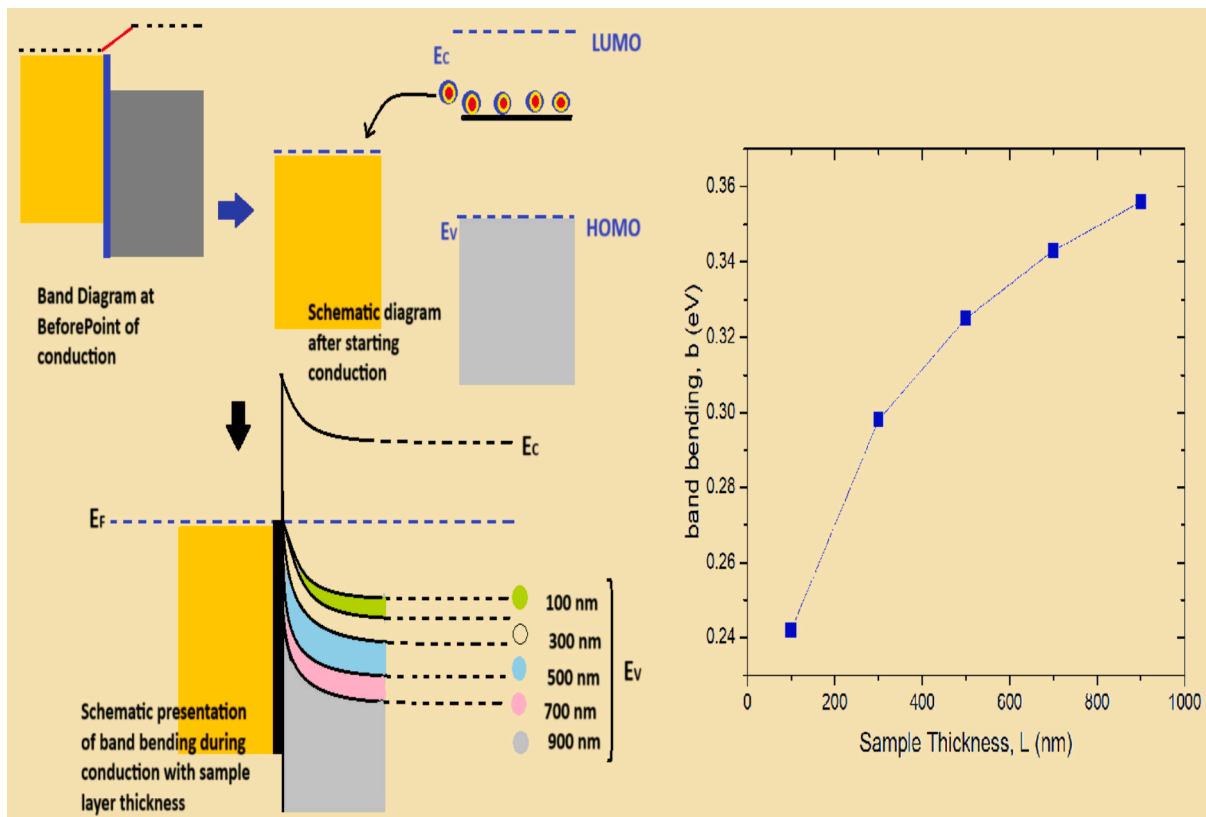

Fig. 4. Schematic representation of band bending during conduction with variation of sample layer thickness. With increasing voltage accumulated carriers starts moving from which band bending becomes dominant due to mismatch of energy band followed by misalignment at Schottky contact. Band bending enhances with increasing thickness offering restriction in charge transition process. b–L plot represents variation bending of energy band varies with the experimental sample thickness. Incremental nature of b is obtained in the mentioned plot under consideration.

the reverse way gradually in this occasion. This carrier transformation process leads to the redistribution of effective barrier potential and b until alignment of Fermi states reforms. According to the investigation of Bruyn et al [27], b can be interpreted by the following equation

$$b = \frac{kT}{q} ln\left[\frac{q^2 N_c L^2}{2exp(2)kT_\epsilon}\right] \tag{2}$$

where k is Boltzmann constant, N_C is the density of states, T is ambient temperature. The standard reported values of required parameters utilized for the b calculation are given as: $N_C = 10^{25}$ m^{-3}, T = 300 k,ϵ is considered 4 and L is varied from 100 nm-900 nm.

During the initiation of voltage execution, Fermi level lies at the middle of the band gap. With increasing voltage, charge transformation starts towards high level of work-function at Schottky regime and subsequently flat band structure faces bending from the interfacial contact. The devices naturally exhibit a cut-off state for positive voltage beyond of which carrier transport improves. Bending of band alignment enhances with increment of the voltage. This consequence has repeated almost similarly for different sample layer thickness. Conductivity can be found to be reduced with high thickness level due to long percolation channel and certain disturbance offered by existing trap states hold between HOMO and LUMO which causes the high value of b what has been estimated from Eq. (2). The results are also validated with our developed theoretical approximation given in Eq. (8). The variation of b with sample thickness has been shown by schematic diagram in Fig. 4.

3.2. Theoretical validation

In order to determine the thickness dependence conduction, both of geometrical conductance (g_m) and mobility (μ) plays a crucial impact. According to Tanase et al [28] and Blom et al [29], charge concentration in organic semiconductors corresponds to carrier mobility follows power law dependence during transition process. In recent observation of Campbell et al [30], charge transition in disordered organic material do not depend on charge density formulation but instead follows the field-based charge mobility. In refer to MG law shown in Eq. (2), mobility can be extracted by the following equation

$$\mu = \frac{8JL^3}{9\epsilon\epsilon_0} \frac{1}{(V - V_{bi})} \tag{3}$$

From the relation of built-in voltage V_{bi} with b and $[CSLEF]_b$ obtained from Wetzalaer's approximation [31] ($\phi_b = V_{bi} + b$), we can modify Eq. (3) such as

$$\mu = \frac{8JL^3}{9\epsilon\epsilon_0} \frac{1}{(V - \phi_b + b)} \tag{4}$$

As it is mentioned above, g_m can be considered to verify the charge tunnelling during penetration through the active regime of the organic device. At higher voltage of V_{bi}, current derivative with respect to voltage denotes g_m. According to Brinkman et al [32], semi parabolic nature of g_m relative to voltage confirms the quantum tunnelling and tendency of charge conduction in different conditions. Hence, differentiating Eq. (2) leads to the mutual relationship of g_m with μ obtained from MG law and gradually b such as

$$\frac{dJ}{d(V - V_{bi})} = \frac{9}{8}\epsilon\epsilon_0\mu\frac{2(V - V_{bi})^2}{L^3} \tag{5}$$

or,

$$g_m = \frac{9}{4}\epsilon\epsilon_0\mu\frac{(V - V_{bi})}{L^3} \tag{6}$$

Hence, in terms of μ, we can rewrite the Eq. (6) in the following way

$$\mu = \frac{9}{4} \frac{L^3}{\epsilon\epsilon_0} \frac{g_m}{(V - V_{bi})} \tag{7}$$

Comparing Eq. (4) and Eq. (7) we obtain

$$\frac{8JL^3}{9\epsilon\epsilon_0} \frac{1}{(V - \phi_b + b)} = \frac{9}{4} \frac{L^3}{\epsilon\epsilon_0} \frac{g_m}{(V - V_{bi})} \tag{8}$$

Solving Eq. (8) we get

$$g_m = \frac{2J}{(V - \phi_b + b)} \tag{9}$$

Therefore,

$$b = \frac{2J}{g_m} + \phi_b - V \tag{10}$$

Considerable asymmetry into the curve appeared due to the work function misalignment of electrodes results band bending which inherently impact upon conductance. The theoretical validation approximated in Eq. (10) indicates that g_m followed by charge tunnelling exhibits decremental tendency with increasing bending of energy bands for all sample thickness which is similar to the observation illustrated in simulation and experimental outcomes of present work.

Distortion driven asymmetry leads to the disturbance formed by trapping states. Trapping defects appeared due to crystallographic defect, grain boundary alignment and conformational bonding defect that occurs in the time of material processing. During the timing of penetration through active regime, the injected carriers suffer by such defected localized states [33]. Carriers getting into the localized sites offered by the traps is released often acquiring required percolation energy or by recombination released energy based on the quantified energy level of different trap centre. Thus, gradually the frequent hopping like carrier movement is offered some serious restriction by the unwanted disordered energy states of traps [34,35]. These localized trap states inherently distributed between HOMO and LUMO, is naturally expected to have a major contribution on disturbance formation in alignment level of bands during charge transition. (From SCLC to TCLC transition, logrithmic I-V relation has been used to find out E_T. (Detail discussion of differential trap energy calculation for all sample thickness has been given in Supplementary File- Pt.3.).

Therefore, it claims to be the matter of concern to critically investigate the impact of trap energy (E_T) on b. There is no theoretical approximation as well as experimental observation are found that relates directly the contribution of E_T on b. Therefore, to have a better solution of this aspect, machine learning (ML) based assessment is introduced in this regard in present report. Detail of ML based predictive modelling of parameter dependence is discussed in next section 3.3.

3.3. Machine learning based approach

To justify the influence of E_T on b, it is essential to develop a reliable predictive model related to charge transition in present obtained observation [15,18,36,37]. In order to comprehend the relationship between the differential E_T and b, machine learning (ML) approaches have been utilized on the Schottky formation for different sample thicknesses while taking simulated samples into consideration. First, the dataset has been created by accumulating the data obtained from simulation environment to determine the E_T and b. Next, the dataset has been divided in an 80:20 ratio between training and test data. Various machine learning algorithms (both Linear and Non-linear ML models) has been trained using the training dataset and subsequently the test dataset has been utilized to obtain various performance measurement metrics. Tables 2 and 3 exhibit the results over various thicknesses for different machine learning models:

Both linear and non-linear regression techniques have been

Table 2

MSE values for different Machine Learning algorithm over various sample thickness (Bold values indicate the best suitable performance of a particular thickness over the trained regressor models under consideration).

ML Trained Models	Sample Thickness				
	100nm	300nm	500nm	700nm	900nm
Random Forest Regressor	1.964415	0.389921	1.329096	**0.005997**	0.008028
AdaBoost Regressor	0.198252	0.03679	1.326853	0.009076	**0.015121**
Linear Regressor	0.309613	0.100809	1.523218	**0.069287**	1.004546
XGB Regressor	0.265681	0.079957	1.355928	**0.006679**	0.033548

employed to examine the dependence of b on E_T across five sample thickness ranges from 100 nm to 900 nm. The model performance on the test dataset was evaluated using the R-Squared ($\mathbf{R^2}$) and Mean Squared Error (MSE) metrics. A higher $\mathbf{R^2}$ value indicates that the model suitably captured the relationship between E_T and b more effectively, while a lower MSE is desirable for better accuracy.

From Tables 2 and 3, it is evident that the relationship between E_T and b is not linear, as the linear models exhibits higher $\mathbf{R^2}$ values and lower MSE compared to non-linear models across different thickness range. Additionally, the machine learning models performed significantly better in modelling this relationship, particularly for the 700 nm thickness. This is perhaps at very low sample thickness-based material, there might be a possibility of short circuit at the contact regime whereas long interaction of drift carrier movement through amorphous penetration channel for very high thickness of sample leads towards reduction in free charges. The meaningful improvement could be attributed to some underlying characteristics at this specific thickness that align better with the model's assumptions.

Based on the trend of the statistical metrics mentioned above, the machine learning models pre-trained on the 700 nm thickness is implemented to predict band bending dependence using experimental

E_T values for both experimental RBD and MRD dye based Schottky contacts as shown in Fig. 5(a) and (b). It was very hard to predict the differential variation of band bending precisely as the experimental observations are not included b, therefore, ML is the only trustable approach to gain better insight upon the dependence of b with trapping distribution. The perspective of insightful realization regarding the arbitrarily distributed trapping sites could be explained by Mobility Edge (ME) [38,46,47] and Multiple trap-releasing (MTR) [39,48] models. Initiating the applicability of both model statements (ME and MTR) can be introduced from amorphous material to an extension of crystalline substances. The similarity of the proposals is found in statement of hopping transitions through the disordered localized states having different energy levels towards extended states. Our trained ML algorithm is highly consistent with the proposal of abovementioned esteemed theoretical approximations. It is clear from the ML based modeling observation, b doesn't follow linearity in terms of E_T as the trained model over linear regressor fails to exhibit any sort of variation of bending of energy bands (in Linear regression model depicted in figure) with respect to increasing trends of energy of distributed trapping sites. At encircled regime depicted in Fig. 5, no significant variation of b is found which concludes non-dependence nature of band bending energy with E_T at point of Schottky contact. This is because change of b is naturally high due to the misalignment of work function at injection regime. In this diffusion dominated regime, carriers start accumulation by injection where density of trapping sites is almost absent [38,40]. Electron Starts hopping between HOMO to LUMO with increasing voltage with a transition to drift dominated domain [41,44,45]. During the penetration by drift hopping zone, carriers meet different distribution of trap energy levels into the same active material. This is mainly SCLC regime where trap concentration is found to be maximum but significant variation of band bending can't be expected during conduction. Bending probability falls by following inverse linearity with increasing E_T in this domain, termed as regime-1. On the other hand, regime-2 denotes the transport energy level beyond SCLC zone where the extended state tends to the formation of hopping to other side of

Table 3

R^2 (R-Squared) values for different Machine Learning algorithm over various sample thickness (Bold values indicate the best suitable performance of a particular thickness over the trained regressor models under consideration).

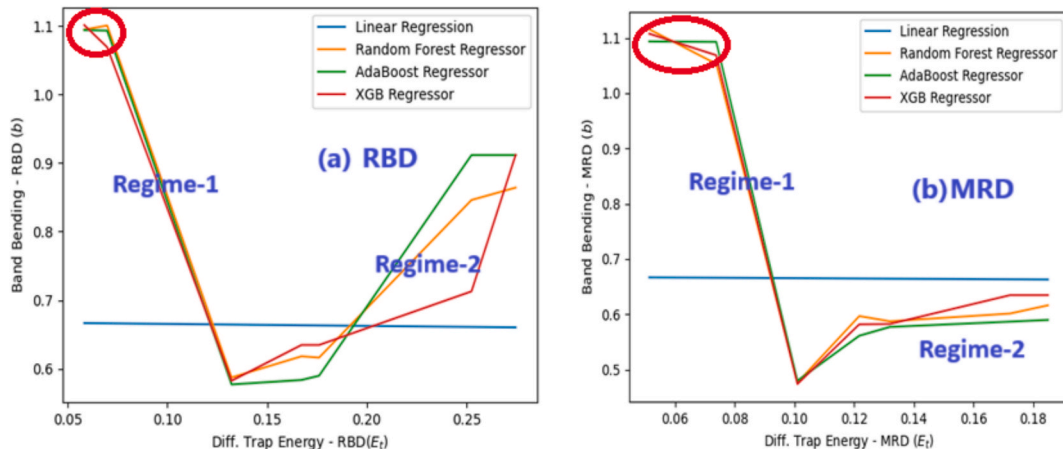| ML Trained Models	Sample Thickness				
	100 nm	300 nm	500 nm	700 nm	900 nm
Random Forest Regressor	−11.5668	−3.5248	0.008496	**0.915236**	0.844372
AdaBoost Regressor	−0.26826	0.573068	0.010169	**0.871711**	0.706877
Linear Regressor	−0.98067	−0.16983	−0.13632	**0.020595**	−18.4737
XGB Regressor	−0.69962	0.07215	−0.01152	**0.905594**	0.349655

Fig. 5. Machine Learning based linear and non-linear dependence of b with variation of E_T for (a) RBD dye-based dye and (b) MRD dye-based device.

contact leading towards transformation of energy band. Relative linearity is expected naturally that results enhancement of b corresponds to inherent distribution of trap states.

4. Conclusion

An analytical approach has been undertaken to verify the impact of b over Vbi and $[CSLEF]_b$. J-V plot obtained by simulated device over the sample thickness ranges between 100 nm to 900 nm has been fitted accordingly and further experimented by RBD and MRD based organic devices. Consistency has been encountered for both simulation and experimental approach. b is found to be increasing with increasing sample thickness. One theoretical approximation has been proposed by introducing modification in empirical Mott-Gurney law to explain the observed consequence relating b in terms of gm. Inverse linearity between the parameters obtained from the developed theoretical relation confirms the validity of the estimated analogy. Machine learning based R2 and Mean Square Error metrics comparison has been employed to determine the precise differential variation of b in terms of ET. Dividing the training and test dataset in 80:20 ratio, execution of different algorithms has been trained and subsequently it is allowed to be utilized to obtain for various performance measurement metrics. The result exhibits its best applicability in 700 nm device thickness, therefore the pretrained models are considered to estimate ET dependent b values for above-mentioned experimental dyes with different linear and non-linear machine learning based regressor models. The outcome of the predictive models confirms non-linear variation of b. In the injection regime, no such relation can be predicted due to less concentration of ET. Drastically inverse linear dependence of b has been observed over SCLC dominated regime where inherent distribution of trapping states is maximum. But all the non-linear models exhibit that variation of b follows linearity with increment of ET beyond SCLC regime in an extended level of conduction towards another electrode contact.

CRediT authorship contribution statement

Kushal Chakraborty: Writing – review & editing, Writing – original draft, Visualization, Validation, Software, Investigation, Formal analysis, Data curation, Conceptualization. **V. Chandrasekar:** Visualization, Software, Investigation, Formal analysis. **Dhananjay Kumar:** Visualization, Validation, Software, Resources, Investigation, Formal analysis. **Nabin Baran Manik:** Writing – review & editing, Supervision, Resources, Formal analysis.

Declaration of competing interest

The authors declare that they have no known competing financial interests or personal relationships that could have appeared to influence the work reported in this paper.

Acknowledgements

Appendix A. Supplementary data

Supplementary data to this article can be found online at https://doi.org/10.1016/j.sse.2025.109144.

Data availability

Data will be made available on request.

References

[1] Varo LP, Tejada JA, Villanueva JA, Deen MJ. Space-charge and injection limited current in organic diode: A unified model. Organic Elec 2014;15(10):2526.

[2] Alver MS, Blom PWM, Wetzalaer GAH. Space-charge-limited electron and hole currents in hybrid organic-inorganic perovskites. Nat Comm 2020;11(4023):1–9.

[3] Zhang P, Zhao S, Wang H, Zhang J, Shi J, Wang H, et al. Relation between Interfacial Band-Bending and Electronic Properties in Organic Semiconductor Pentacene. Adv Elec Mat 2017;3. 1700136(1–6).

[4] Wang H, Yan D. Organic hetero-structures in organic field-effect transistors. NPG Asia Mat 2010;2:69–78.

[5] Fung M, Li Y, Liao L. Tandem Organic Light-Emitting Diodes. Adv Mat 2016;28 (47):10381–408.

[6] Vazquez H, Skouta R, Schneebeli S, Kamenetska M, Breslow R, Venkatraman L, et al. Probing the conductance superposition law in single-molecule circuits with parallel paths. Nat Nanotech 2012;7:663–7.

[7] Winkler S, Amsalem P, Frisch J, Oehzelt M, Heimel G, Koch N. Probing the energy levels in hole-doped molecular semiconductors. *Mater Horiz* 2015;2:427–33.

[8] Oehzelt M, Koch N, Heimel G. Organic semiconductor density of states controls the energy level alignment at electrode interfaces. *Nat Comm* 2014;18(5):4174.

[9] Malliaras GG, Salem JR, Brock PJ, Scott JC. Photovoltaic measurement of the built-in potential in organic light emitting diodes and photodiodes. *J Appl Phys* 1998;84: 1583.

[10] Röhr JA, Shi X, Haque SA, Kirchartz T, Nelson J. Charge Transport in Spiro-OMeTAD Investigated Through Space-Charge-Limited Current Measurements. *Phys Rev Appl* 2018;9:044017.

[11] Campbell IH, Hagler TW, Smith DL, Ferraris JP. Direct Measurement of Conjugated Polymer Electronic Excitation Energies Using Metal/Polymer/Metal Structures. *PhysRevLett* 1996;76:1900.

[12] Röhr JA. Direct Determination of Built-in Voltages in Asymmetric Single-Carrier Devices. *Phys Rev* 2019;11:054079.

[13] Mensfoort SLM, Coehoorn R. Determination of Injection Barriers in Organic Semiconductor Devices from Capacitance Measurements. *Phys Rev Lett* 2008;100 (8):086802.

[14] Shi X, Nádaždy V, Perevedentsev A, Frost J, Wang X, von Hauff E, et al. Relating Chain Conformation to the Density of States and Charge Transport in Conjugated Polymers: The Role of the β-phase in Poly(9,9-dioctylfluorene). *Phys Rev X* 2019;9 (2):021038.

[15] Salvy N, Klymenko M, Christofferson A, Bach U, Winkler D, Russo P. Machine learning property prediction for organic photovoltaic devices. *npj Comp Mat* 2020;6 (166):1–8.

[16] Padula D, Simpson JD, Troisi A. Combining electronic and structural features in machine learning models to predict organic solar cells properties. *Mater Horiz* 2019;6:343–9.

[17] Altman NS. An introduction to kernel and nearest-neighbour nonparametric regression. *Am Stat* 1992;46:175–85.

[18] Vu K, et al. Understanding kernel ridge regression: common behaviours from simple functions to density functionals. *Int J Quant Chem* 2015;115:1115–28.

[19] Rupp M. Machine learning for quantum mechanics in a nutshell. *Int J Quant Chem* 2015;115:1058–73.

[20] Sahu H, Rao W, Troisi A, Ma H. Toward predicting efficiency of organic solar cells via machine learning and improved descriptors. *Adv Energy Mater* 2018;8:1801032.

[21] Pereira V, et al. Machine learning methods to predict density functional theory B3LYP energies of HOMO and LUMO orbitals. *J Chem Inf Model* 2016;57:11–21.

[22] Mishra A, Shukla R. Electrical and optical simulation of typical perovskite solar cell by GPVDM software. *Mat Today Proc* 2022;49(8):3181–6.

[23] Chakraborty K, Mandal R, Das A, Mondal DK. A unified realization of the modified Einstein equation approach in organic semiconductors: theoretical interpretation and experimental validation. *Ind J Phys* 2023;97:3033–40.

[24] Chakraborty K, Chakraborty S, Manik NB. Effect of single walled carbon nanotubes on series resistance of Rose Bengal and Methyl Red dye-based organic photovoltaic device. *J Semicon* 2018;39(9). 094001(1–7).

[25] Watzelaer GAH. Improved determination of the mobility and built-in voltage in asymmetric single-carrier devices. *Phys Rev Appl* 2020;13. 034069(1–5).

[26] Pil'nik AA, Chernov AA, Islamov DR. Charge transport mechanism in dielectrics: drift and diffusion of trapped charge carriers. *Sci Rep* 2020;10:15759.

[27] Bruyn P, Rest AHP, Wetzelaer LDM, Blom PWM. Diffusion-limited current in organic Metal-Insulator-Metal diodes. *Phys Rev Lett* 2013;111:186801.

[28] Tanase C, Meijer EJ, Blom PWM, De Leeuw DM. Unification of the hole transport in polymeric field-effect transistors and light-emitting diodes. *Phys Rev Lett* 2003;91 (21):216601.

[29] Blom PWM, Tanase C, de Leeuw DM, Coehoorn R. Thickness scaling of the space-charge limited current in poly (p-phenylene vinylene). *Appl Phys Lett* 2005;86(9): 092105.

[30] Campbell AJ, Rawcliffe R, Guite A, Faria JCD. Charge carrier density independent mobility in amorphous fluorene-triarylamine copolymers. *Adv Func Mat* 2016;26 (21):3720.

[31] Wetzelaer GAH. Improved Determination of the Mobility and Built-In voltage in Asymmetic Single-Carrier Device. *Phys Rev Appl* 2020;13:034069.

[32] Brinkman WF, Dynes RC, Rowell JM. Tunnelling conductance of Asymmetrical barriers. *J Appl Phys* 1970;41(5):1915.

[33] Haneef HF, Zeidell AM, Jurchescu OD. Charge carrier traps in organic semiconductors: a review on the underlying physics and impact on electronic devices. *J Mater Chem C* 2020;8:759.

[34] Baranovskii SD, Cordes H, Hensel F, Leising G. Charge-carrier transport in disordered organic solids. *Phys Rev B* 2000;62(12):7934.

[35] Mott NF, Gurney RW. *Electronics process in ionic crystals*. Oxford: Oxford University Press; 1948.

[36] Bozyigit D, Lin MMW, Yazdani N, Yarema O, Wood V. A quantitative model for charge carrier transport, trapping and recombination in nanocrystal-based solar cells. *Nature Comm* 2014;6(6180):1–10.

[37] Ran NA, et al. Charge generation and recombination in an organic solar cell with low energetic offsets. *Adv Energy Mater* 2018;8:1701073.

[38] Cottaar J, Coster L, Coehoorn R, Bobbert P. Scaling theory for percolative charge transport in disordered molecular semiconductors. *Phys Rev Lett* 2011;107:136601.

[39] Felekidis N, Melianas A, Kemerrink M. Non-equilibrium drift-diffusion model for organic semiconductor devices. *Phys Rev B* 2016;94:035205.

[40] Chakraborty K, Das A, Mandal R, Mandal DK. Investigation on the Trap Signature in Organic Semiconductor Turmeric Film Through Current–Voltage Analysis. *Trans Tianjin Univ* 2020;26:265–72.

[41] Chakraborty K, Das A, Mandal R, Mandal DK. Interpretation of trap-assisted conduction with estimation of electrical parameters of thin indigo film-based semiconducting device. *Bull Mat Sci* 2021;44:92.

[42] Kumar D, Bhowmick P, Dey S, Sanyal D. On the banks of Shodhganga: analysis of the academic genealogy graph of an Indian ETD respiratory. *Scientomet* 2023;128 (1):3879.

[43] Kumar D, Bhowmick P, Paik J. Researcher Influence Prediction (Resip) Using Academy Genealogy Network. *J Informatics* 2022;17(2):101392.

[44] Shah M, Karimov KS, Ahmad Z, Sayyad M. Electrical characteristics of Al/CNT/ NiPc/PEPC/Ag surface-type cell. *Chin Phys Lett* 2010;27(10):106102.

[45] Chakraborty K, Das A, Mandal R, Mandal DK. An analytical study on low voltage regime of natural organic semiconductor-based device: Physics of trap energy and ideality factor. *Sol Comm* 2021;323:114080.

[46] Wang W, et al. Organic Photodetectors with Gain and Broadband/Narrowband Response under Top/Bottom Illumination Conditions. *Adv Opt Mat* 2018;6(216): 1800249.

[47] Zhao Z, et al. Ultraviolet Narrowband Photomultiplication Type Organic Photodetectors with Fabry−Pérot Resonator Architecture. Adv Func Mat 2022;32 (29):2203606.

[48] Zhao X, et al. Narrowband Organic Photodetectors: From Fundamentals to Prospects. *Adv Opt Mat* 2024;12(31):2401087.